Crystallographic Orientation of Orthorhombic Aragonite using reflection generalized ellipsometry

G. E. Jellison, Jr.[1], D. N. Leonard[1], L. M. Anovitz[2], M. Cheshire[2], E. D. Specht[1] and T. M. Rosseel[1]

[1]Materials Science and Technology Division, Oak Ridge National Laboratory, Oak Ridge, TN 37831, USA

[2]Chemical Sciences Division, Oak Ridge National Laboratory, Oak Ridge, TN 37831, USA

ABSTRACT

The 2-modulator generalized ellipsometry microscope (2-MGEM) has been used to study a natural crystal of aragonite. Like its polymorph calcite, aragonite has a large refractive index difference between light polarized parallel to the c-axis and light polarized perpendicular to the c-axis. Unlike calcite, aragonite is orthorhombic, so there also is a very small difference between the refractive indices polarized along the a- and b-directions. As a result, it is not possible to use the 2-MGEM to obtain a definitive map of the optic axis directions of a sample as was possible with calcite, but it is possible to determine approximately the orientation of the c-axis with respect to the surface normal. If the c-axis is in the sample surface plane, it is possible to measure very small deviations of the c-axis direction with an accuracy of ~0.2°. If the c-axis is oriented normal to the sample surface, 2-MGEM data can be used to identify different crystallites due to rotations about the c-axis. For comparison, the orientations of some of the crystallites have also been measured using x-ray Laue and electron beam backscatter diffraction (EBSD). In addition, spectroscopic generalized ellipsometry measurements have been used to determine the refractive indices of aragonite.

I. INTRODUCTION

Calcium carbonate ($CaCO_3$) is a common material found throughout the earth's crust. The most common phase is calcite, which is trigonal and therefore optically uniaxial. Other naturally occurring polymorphs of $CaCO_3$ include aragonite and vaterite, which have the same chemical composition but different crystal structures. Aragonite is orthorhombic, whereas vaterite is hexagonal. Both polymorphs can be created from either physical or biological processes, but aragonite is much more common since it is considerably more stable than vaterite (Chang et. al, 1995, Davis and Adams, 1965, Christy, 2017). Aragonite is named for the Molina de Aragón region in Castilla-La Mancha, Spain, but has been found in many other places around the globe. It can be formed either geologically under high temperature and pressure or biologically, as it is found naturally in the shells of many mollusks (Meldrum, 2003 and Morse et. al 2007). Under the temperature and pressure conditions at the earth's surface, aragonite will transform to calcite in 10^4 to 10^8 years (Davis and Adams, 1965; Huang, 2003). Because of its relationship to calcite, aragonite is an important geological material, but its importance extends beyond geological systems. As discussed in a previous paper (Jellison et al, 2018), $CaCO_3$ is also one of several primary constituents of concrete aggregates, which can degrade in nuclear environments due to neutron-induced swelling and subsequent cracking. Efforts to evaluate these radiation effects under controlled conditions on mineral analogues of concrete aggregates (Rosseel et al, 2017 and Silva et al, 2018) and to combine optical and X-ray microscopy mapping of minerals in concrete aggregates to identify crystal boundaries and orientations are underway (Le Pape et al., 2019) and are critical to understanding radiation-induced micro cracking reactor cavity concrete.

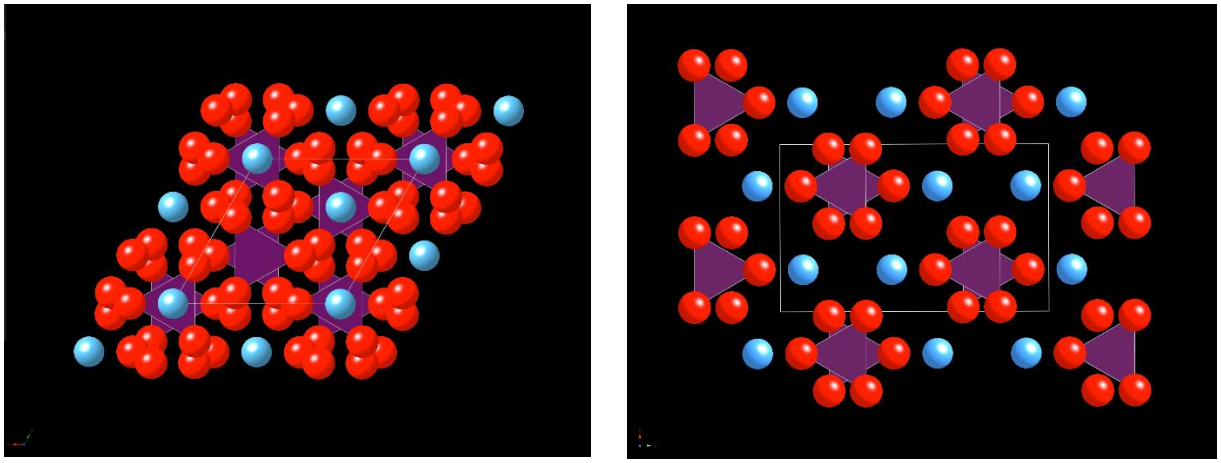

Figure 1. Structural diagram of calcite (left) and aragonite (right), where the c-axis is pointed out of the page. The red balls represent the oxygen atoms, the blue balls the calcium atoms and the purple triangles indicate the CO_3 units.

Structurally, both calcite and aragonite consist of planar CO_3 units that are preferentially aligned in the crystal structure (Figure 1). In calcite, these CO_3 units are aligned such that the crystal has three-fold rotational symmetry about the axis perpendicular to the plane of the CO_3 units, while the crystal structure of aragonite results in two-fold rotational symmetry about three axes, making the material orthorhombic, but the CO_3 units are all aligned in a common direction. In both cases, the refractive index for light

polarized along the axis perpendicular to the plane of the CO_3 units [001] is considerably less than that for light polarized parallel to the plane of the CO_3 units, making both materials negatively birefringent. (Bragg, 1924). The unit cell of aragonite consists of 4 $CaCO_3$ units with point group mmm (Schönflies D_{2h}) and space group Pmcn with unit cell dimensions: a = 0.495 nm, b = 0.796 nm, and c = 0.574 nm. As a result, the angle between the [110] and [1-10] directions are 63.8°. This is very close to 60°, so aragonite is often considered to have a distorted hexagonal structure. This is supported by the pseudo-hexagonal shape of many of the aragonite crystals. Optically, the refractive indices for light polarized along [100] (a-direction) is nearly the same as that for light polarized along [010] (b-direction), making aragonite nearly uniaxial (Bragg, 1924).

In a previous paper, we have already shown that reflection generalized ellipsometry can be used to characterize mixed crystals of the related materials calcite and dolomite ($CaMg(CO_3)_2$, Jellison, et. al. 2018). Since both materials are uniaxial, the generalized ellipsometry results have been used to determine the optical pole figure of the of a sample. That is, for each observable crystallite, one can determine the diattenuation and the direction of the principal axis which can then be used to determine the direction of the optic axis with respect to the sample surface.

In this paper, the results from reflection generalized ellipsometry of naturally formed aragonite will be presented and discussed. To complement the results from reflection generalized ellipsometry, spectroscopic generalized ellipsometry results will be used to determine the refractive indices of the material. Since aragonite is orthorhombic, the three principal axes are determined from the symmetry of the crystal and are mutually orthogonal. As a result, it is not possible to measure an optical pole figure such as was done with higher-symmetry calcite crystallites. However, the optical results do show the crystallites and grain boundaries, and the orientations of the crystallites can be constrained. Results from electron backscatter diffraction (EBSD) and X-ray Laue measurements will also be shown as independent checks on the optical results.

II. EXPERIMENTAL

A. Sample

A polycrystalline sample from the type location for aragonite, the Molina de Aragón region, Province of Guadalajara in Castilla-La Mancha, Spain was used for these studies (Figure 2). Due to its pseudohexagonal structure, aragonite naturally twins to give the appearance of a hexagonal crystal, where the c-axes (the axis of low refractive index) of the crystallites are preferentially aligned. This sample was cut into 4 pieces, one that had the c-axis perpendicular to the surface plane of the sample (c-perp) and 3 where the c-axis was nominally parallel to the sample surface and cut to expose 3 of the pseudo hexagonal faces of the crystal (S1, S2, and S3). The top surface of each sample

Figure 2. Photograph of an aragonite crystal from the Molina de Aragón mine.

was then optically polished, using a vibratory polishing machine with a suspension of 50% colloidal silica and 50% distilled water as the final step. Some of the sample was also ground into a powder to perform x-ray powder diffraction measurements to confirm its mineralogy. These results showed that the sample was ~98% aragonite and 1-2% gypsum. No calcite was detected.

X-ray backscatter Laue measurements were also performed to determine the direction of the axes of each sample. The Laue measurements affirmed that the sample was orthorhombic, with a distorted hexagonal structure with the angle between [110] and [1-10] being 63°. The x-ray spot size was ~1 mm, over which no twinning was observed. The measured c-axis of the c-perp sample was 0.7° off normal at the x-ray spot measured, while the [110] directions of the 3 other samples were off normal by 3.9°(S1), 3.1°(S2), and 1.2°(S3), respectively.

B. Spectroscopic Generalized Ellipsometry

Table I. Fitting results from the spectroscopic ellipsometry measurements on two samples of aragonite with the c-axis parallel to the sample surface using the uniaxial and orthorhombic models of the crystals. The refractive indices as calculated from these parameters at 589 nm are also shown, as well as the diattenuation N calculated at 577 nm. For the uniaxial model, only a single diattenuation is calculated, while two values of the diattenuation are calculated for the orthorhombic model.

Parameter	S1 Uni	S1 Ortho	S2 Uni	S2 Ortho
Rough Thick (nm)	1.24±0.06	1.24±0.06	1.40±0.05	1.40±0.05
A_e	1.199±0.002	1.198±0.002	1.208±0.002	1.207±0.002
$\lambda_{,e}$	99.4±0.9	99.5±1.1	99.8±1.0	99.8±1.0
A_o	1.602±0.003	1.604±0.004	1.615±0.003	1.623±0.004
$\lambda_{o,o1}$	120.1±0.9	120.7±1.2	119.4±0.8	120.2±1.3
A_{o2}	----	1.596±0.004	----	1.603±0.004
$\lambda_{o,o2}$	----	119.7±1.3	----	118.8±1.3
χ^2	1.38	1.36	1.12	1.04
n_e (589 nm)	1.495±0.001	1.494±0.001	1.498±0.001	1.498±0.001
n_{o1} (589 nm)	1.635±0.001	1.635±0.001	1.638±0.001	1.641±0.002
n_{o2} (589 nm)	----	1.632±0.002	----	1.634±0.002
N1 (577 nm))	0.192±0.002	0.194±0.002	0.192±0.002	0.195±0.002
N2 (577 nm))	----	0.190±0.002	----	0.188±0.002

Generalized ellipsometry measurements were performed using the two-modulator generalized ellipsometer (2-MGE) (Jellison and Modine, 1997) on samples S1 and S2 where the c-axis is nearly parallel to the sample surface. As described in more detail in Jellison et. al. 2018, four (4) spectroscopic generalized ellipsometry measurements were performed from 220 to 850 nm, with the c-axis oriented at 90°, 45°, 0°, and -45° with respect to the reference frame of the ellipsometer. These data were analyzed by fitting the spectra simultaneously to a simple structure consisting of air/roughness/crystal, where the optical functions of the crystal were modeled using the Sellmeier approximation:

$$n^2(\lambda) = \varepsilon(\lambda) = 1 + \frac{A\lambda^2}{\lambda^2 - \lambda_o^2} \qquad (1)$$

where n is the refractive index, ε is the dielectric function, λ is the wavelength of light (in nm), A is the amplitude of the oscillator and λ_o is the wavelength of the resonance (Jellison, 1993, 1998). The ellipsometry data from samples S1 and S2 were fit using the both the uniaxial and orthorhombic models, where the orthorhombic model assumed that the [110] axis was normal to the sample surface. The results of the fits are shown in Table I, including the reduced χ^2 which indicates that the models fit the data.

C. Reflection Generalized Ellipsometry

Two-modulator generalized ellipsometry microscope (2-MGEM) measurements were made on the four samples described in Jellison, et. al (2006) and Jellison et. al. (2018). The instrument operates at 577 nm in reflection mode, with an analysis spot size of ~5-6 microns. Because of the design of the instrument, the collection cone for light reflected from the sample surface is quite small (f-number ~12). Any light reflected out of the collection cone will not affect the measurement other than reducing the signal to noise ratio.

Several parameters were measured at each measurement point, but the most important ones are the diattenuation N and the direction of the principal axis γ with the degree of depolarization β being used as a measure of the quality of the data. The diattenuation N is a function of the light polarization direction and is given by $N = (R_{max} - R_{min}) / (R_{max} + R_{min})$ where R_{max} and R_{min} are the maximum and minimum reflectivities of the sample as a function of the polarization direction of the incident light. This will be 0 for light reflected off an isotropic sample or a uniaxial sample with the optic axis perpendicular to the sample surface. The principal angle γ is the angle of light polarization that gives maximum reflectivity with respect to the reference frame of the 2-MGEM. Note that the transformation N=> -N, and γ => γ+90° does not change the measured Mueller matrix elements and is also an allowed solution.

If the depolarization fraction is significantly different from 0 then the sample is depolarizing the light beam and the measurement should not be considered valid. This depolarization can originate from several causes, including the presence of multiple crystallites within the measured spot size, light reflected off a sub-surface feature, very low reflected light intensity, etc.

D. Electron Backscatter Diffraction (EBSD)

Electron backscatter diffraction (EBSD) has long been used for the determination of crystal structure in rocks (Prior et. al 1999). To compare 2-MGEM with EBSD, several regions of the c-perp sample were examined by both 2-MGEM and EBSD, where the EBSD was performed using a JEOL JSM-6500F scanning electron microscope with an EDAX Hikari EBSD attachment. The data were analyzed using the EDAX-OIM version 7.2 analysis software package. The SEM was operated at 20 KV and 4 nA beam current, while the

EBSD camera operated at 2 X 2 binning with 32 X 240 binned pixels. Each pixel was averaged from 5 patterns. Since aragonite is insulating, it was necessary to coat the sample with a thin layer of carbon prior to measurement to minimize charging.

III. THEORY: DIATTENUATION AND PRINCIPAL AXIS DIRECTION AT NORMAL INCIDENCE

At normal incidence, light reflected from an isotropic sample will be have no polarization dependence. The diattenuation will be 0 and the direction of the principal axis will be indeterminate. If the sample is anisotropic, then the light reflection may depend upon the polarization of the light and analysis yields a diattenuation and a direction of the principal axis. To calculate this, one uses the formalism of Berreman (1972) as discussed in Jellison et. al (2011). The dielectric tensor for a randomly oriented orthorhombic crystallite is given by

$$\varepsilon = \begin{bmatrix} \varepsilon_{11} & \varepsilon_{12} & \varepsilon_{13} \\ \varepsilon_{12} & \varepsilon_{22} & \varepsilon_{23} \\ \varepsilon_{13} & \varepsilon_{23} & \varepsilon_{33} \end{bmatrix} = A(\theta,\phi,\psi) \begin{bmatrix} \varepsilon_a & 0 & 0 \\ 0 & \varepsilon_b & 0 \\ 0 & 0 & \varepsilon_c \end{bmatrix} A^T(\theta,\phi,\psi) \qquad (2)$$

Where A(θ, ϕ, ψ) is the Euler transformation matrix for the Euler angles θ, ϕ, and ψ and ε_a, ε_b, and ε_c are the dielectric functions for light polarized along the a [100], b [010], and c [001] principal directions. The optical reflection from this crystallite is determined from the Berreman matrix Δ. At normal incidence, some of the elements of the Berreman matrix go to 0 or 1, giving

$$\Delta = \begin{bmatrix} 0 & 1 & 0 & 0 \\ \Delta_{21} & 0 & \Delta_{23} & 0 \\ 0 & 0 & 0 & 1 \\ \Delta_{23} & 0 & \Delta_{43} & 0 \end{bmatrix} \qquad (3)$$

where the components of the Berreman matrix are given in terms of the rotated dielectric tensor:

$$\Delta_{21} = \varepsilon_{11} - \frac{\varepsilon_{13}^2}{\varepsilon_{33}} \qquad (4a)$$

$$\Delta_{23} = \varepsilon_{12} - \frac{\varepsilon_{13}\varepsilon_{23}}{\varepsilon_{33}} \qquad (4b)$$

$$\Delta_{43} = \varepsilon_{22} - \frac{\varepsilon_{23}^2}{\varepsilon_{33}} \qquad (4a)$$

The positive eigenvalues of Δ (for reflected waves) are given by

$$\lambda_1 = \frac{1}{\sqrt{2}}\sqrt{\Delta_{21} + \Delta_{43} + Q} \qquad (5a)$$

$$\lambda_3 = \frac{1}{\sqrt{2}}\sqrt{\Delta_{21} + \Delta_{43} - Q} \qquad (5b)$$

where

$$Q = \sqrt{(\Delta_{21} - \Delta_{43})^2 + 4\Delta_{23}^2} \qquad (5c)$$

After some calculation, the diattenuation and direction of the principal axis are given by:

$$|N| = \frac{2(\lambda_1 - \lambda_3)(\lambda_1\lambda_3 - 1)}{(\lambda_1 - \lambda_3)^2 + (\lambda_1\lambda_3 - 1)^2} \qquad (6a)$$

$$\tan(2\gamma) = \frac{sin(2\gamma)}{cos(2\gamma)} = \frac{2\Delta_{23}}{-(\Delta_{21} - \Delta_{43})} \qquad (6b)$$

Obviously, the measurement of the diattenuation and principal axis angle is not sufficient to determine both the values of ε_a, ε_b, and ε_c and the values of the Euler angles θ, ϕ, and ψ. Even if the values of ε_a, ε_b, and ε_c are known, there still is not sufficient data to determine the Euler angles θ, ϕ, and ψ for a general orientation of the crystal. However, measurements of N and γ can be useful in constraining the values of the Euler angles.

IV. RESULTS AND DISCUSSION

A. Spectroscopic Generalized Ellipsometry

Table I shows the resulting fits for two sets of 2-MGE data. Each data set was fit using both the uniaxial and orthorhombic models where the [110] direction is perpendicular to the sample surface. As can be seen from the χ^2 values obtained, the orthorhombic model is only marginally better than the uniaxial model, and all of the χ^2 values are near 1 and therefore acceptable. Moreover, the resulting refractive indices n_{o1} and n_{o2} are very close, and the average is the same as the ordinary refractive index n_o obtained from the uniaxial fit. Thus, the spectroscopic ellipsometry results of aragonite show that it is nearly uniaxial, consistent with its known structure.

Unfortunately, there do not appear to be any recent data in the literature with which to compare these results. The only values that could be found for the refractive indices can be attributed to W. L. Bragg (1924), in which values of 1.530, 1.681, and 1.686 are quoted as the refractive indices at 589 nm of the three principal directions of aragonite. These values are considerably higher than the values that are quoted in Table I. Unfortunately, the Bragg paper does not contain any discussion about the measurement technique used nor the origin of the sample, so a proper comparison of the data cannot be made.

There are at least two factors that could result in a lower refractive index resulting from an ellipsometry measurement. First, the refractive index measured by ellipsometry only gives the refractive

index at the sample surface; if the refractive index changes slowly from the bulk to the surface, the value at the surface is the quantity measured by ellipsometry (Jellison, 1993, 1998). (Surface roughness does not affect the measurement in the same way since the change in refractive index with depth is much larger.) Secondly, as is typical for natural materials, the crystals measured are quite imperfect, with inclusions and voids, both of which may lower the refractive index. (Recall that x-ray powder measurements found 1-2% gypsum in these samples.)

At normal incidence, anisotropic materials may exhibit a diattenuation N. For uniaxial crystals

$$|N| = \left|\frac{R_e - R_o}{R_e + R_o}\right| = \frac{2\varsigma}{1+\varsigma^2} \qquad (7a)$$

$$\varsigma = \frac{|n_e - n_o|}{n_o n_e - 1} \qquad (7b)$$

where R_e (R_o) is the reflectivity for light polarized parallel (perpendicular) to the optic axis (See Jellison et. al 2018), and n_e (n_o) is the refractive index in the same direction. The maximum diattenuation occurs when the optic axis is parallel to the sample surface. Using the refractive indices shown in Table I, one maximum diattenuation can be calculated for the uniaxial approximation, and two for the orthorhombic approximation, one for n_{o1} and one for n_{o2}. If the refractive indices obtained by Bragg (1924) are used, then N1 = 0.1956, N2=0.1904, with an average value of 0.1930. Thus, within the error of the ellipsometry measurements, the Bragg diattenuations are the same as the results in Table I. The small difference between N1 and N2 is to be expected for an orthorhombic material that is nearly uniaxial.

Geologists often characterize biaxial crystals by their 2V angle, which is the angle between the two optic axes in the crystal. This parameter can be calculated from the measured refractive indices as

$$2V = 2 * \text{atan}\left[\sqrt{\frac{n_c^2(n_a^2 - n_b^2)}{n_a^2(n_b^2 - n_c^2)}}\right] \qquad (8)$$

where the refractive indices for light polarized along the principal axes are ordered either as $n_a > n_b > n_c$ or $n_a < n_b < n_c$. The 2V from Bragg's refractive indices is 19.2°±3.4° (assuming an error of the refractive indices of 0.001), while the 2V from sample S1 is 15.6°±9.7° and 23.9°±6.1° from sample S2 (See Table I for the values of n and errors). The generally accepted 2V angle is 18° (Chang et. al, 1995, Troeger, 1979), which agrees with all measurements.

B. 2-MGEM measurements with the c-axis parallel to the sample surface

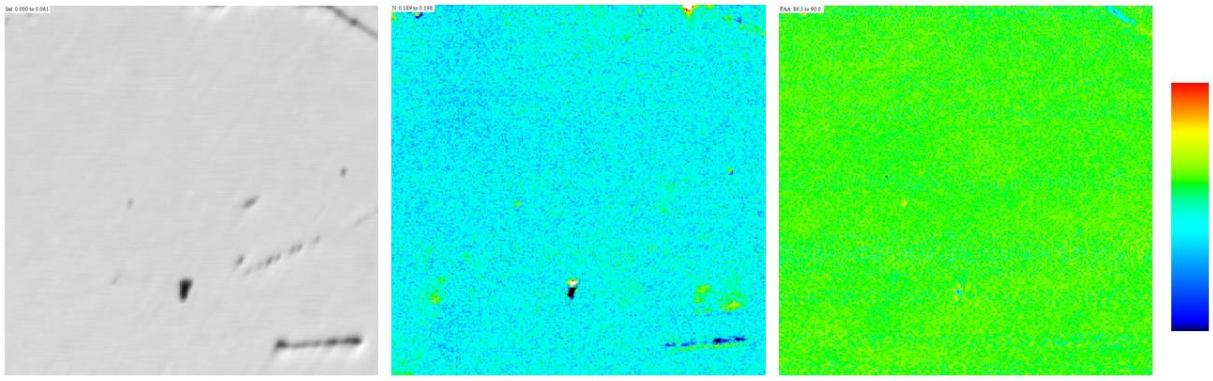

Intensity (0 – 0.061) Diattenuation (0189 – 0.198) Principal Angle (87.7° to +91.4°)

Figure 3. 2-MGEM data from sample S2 taken near the spot sampled by the Laue x-ray measurement. The color scale is to the right and the values in parentheses give the ranges. The scale is 1.31 X 1.29 mm.

Table II. Comparison of 2-MGEM measurements of the pristine regions and X-ray Laue measurements. The measured quantities from Laue are the angle of the a-b plane, which compares directly with the angle γ measured using the 2-MGEM.

	S1	S2	S3
2MGEM γ	89.8°±0.2°	89.9°±0.2°	91.0°±0.2°
2MGEM N	0.1937±0.0008	0.1923±0.0006	0.1914±0.0008
Laue $\perp$ c-axis	86.1°	93.1°	88.8°
Laue c-axis $\angle$ normal θ	92.6°	94.1°	94.6°
Calculated Diattenuation	0.1916	0.1910	0.1908

Three samples (S1, S2, and S3) were cut parallel to the pseudo-hexagonal faces of the natural crystal. These faces were optically polished and 2-MGEM measurements were made on several areas of the exposed surface. One region of each crystal was chosen where there were no observable grain boundaries so that 2-MGEM and X-ray Laue measurements could be made on the same spot. The 2-MGEM data from one of these regions from sample S2 is shown in Figure 3. In these pristine regions, the 2-MGEM measured the diattenuation N and direction of the principal axis γ while the X-ray Laue measurements determined the actual crystallographic directions. Both experiments measure the angles with respect to their own laboratory reference frame, which may vary by 2-3° depending on sample placement. The error quoted for the 2-MGEM γ measurement is relative to the sample only and does not include the systematic error from sample placement.

The principal axis angle γ as determined from 2-MGEM measurements can be compared directly with the measured value of the perpendicular to the c-axis as measured by X-ray Laue. As can be seen from Table II, these measurements agree within the systematic error of sample placement for each of the three samples.

For uniaxial crystals, (Jellison et. al 2018),

$$N = N_{max} sin^2(\theta) \qquad (9)$$

where the angle θ corresponds to the angle of the optic axis with respect to the sample normal. Maximum diattenuation occurs when the optic axis is parallel to the sample surface. Since the aragonite samples examined are nearly uniaxial and the [110] axis is nearly perpendicular to the sample surface, N_{max} = 0.192; this is just the value that is obtained from the uniaxial model or the average (N1+N2)/2 from the orthorhombic model. (Bragg's (1924) data yields N_{max} = 0.193 at 589 nm.) Using Equation 9 and the angle θ determined from Laue, the calculated diattenuation can be determined and is shown in Table II. The agreement between the three samples is quite good, although all three are slightly lower than that calculated from the data of Bragg (1924).

Table III. values of the diattenuation N and direction of the principal axis γ for the regions indicated in Figure 4.

Region	N	γ
S1 a	0.1936±0.0011	92.0°±0.2°
S1 b	0.1938±0.0008	92.8°±0.3°
S1 c	0.1934±0.0008	90.1°±0.2°
S2 a	0.1915±0.0008	88.3°±0.2°
S2 b	0.1916±0.0018	89.1°±0.2°
S2 c	0.1903±0.0034	88.5°±0.2°
S3 a	0.1900±0.0011	91.8°±0.2°
S3 b	0.1894±0.0011	92.4°±0.2°
S3 c	0.1891±0.0013	93.5°±0.2°

Most regions of samples S1, S2, and S3 were not composed of large, pristine single crystals but contained observable grain boundaries. Figure 4 shows regions from all three samples that include one or more grain boundaries. Three such sub-regions from each sample were selected for further analysis, as indicated by the circled letters in Figure 4, and the resulting data are shown in Table III. The values of the diattenuation are nearly the same for each region within the sample, which indicates that the direction of the c-axis with respect to the sample normal is nearly the same for the area sampled. However, the direction of the principal axis can change depending upon the region. Recall that the measurement of the relative direction of the principal axis is not dependent upon sample placement. This change is small, but well outside the error limits of the measurement. This shows that the 2-MGEM is very sensitive to small changes in crystallite orientation if the diattenuation is reasonably large. Furthermore, rotations of the crystallite about the c-axis would marginally change the measured diattenuation but not change the direction of the principal axis. This observed variation of the principal axis is due to small variations in the direction of the c-axis; showing that natural aragonite has many small-angle grain boundaries.

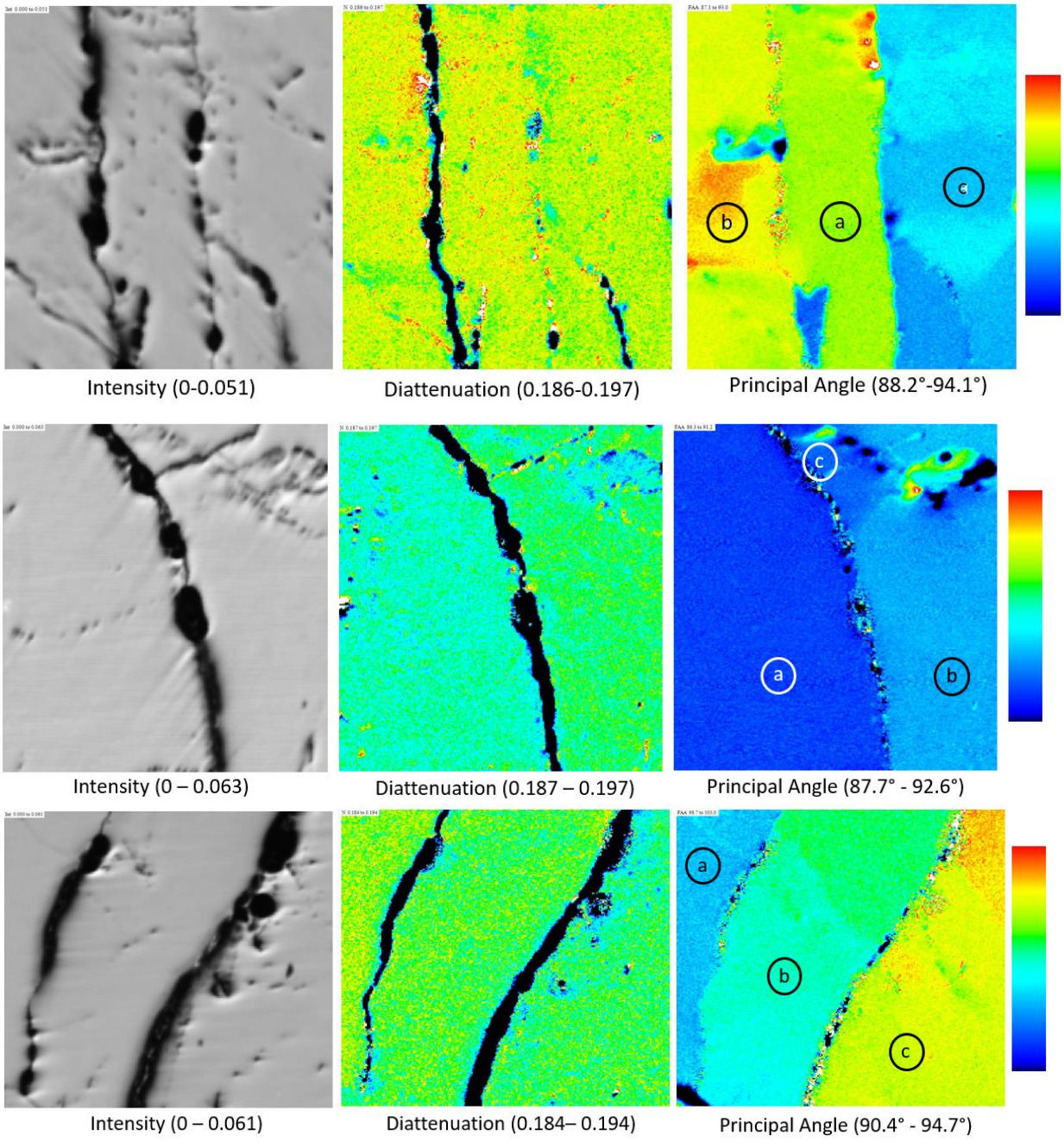

Figure 4. 2-MGEM data from sample S1 (top), S2 (middle) and S3 (bottom) taken in regions near a grain boundary. The color scale is to the right and the values in parentheses give the ranges. The scale is 1.12 X 1.24 mm for S1 (top), 1.185 X 1.265 mm. for S2 (middle) and 1.24 X 1.12 mm for S3 (bottom)

C. 2-MGEM and EBSD measurements with the c-axis perpendicular to the sample surface

One sample was cut such that the c-axis was nearly perpendicular to the sample surface. This sample was examined using 2-MGEM, X-ray Laue and EBSD. Three regions from this sample are shown in Figures 5, 6 and 7. The average values of the diattenuation and the direction of the principal axis γ for each of the subregions notated by the circled letters are given in Table III. The data presented represents a subset of the 7 regions measured on this sample.

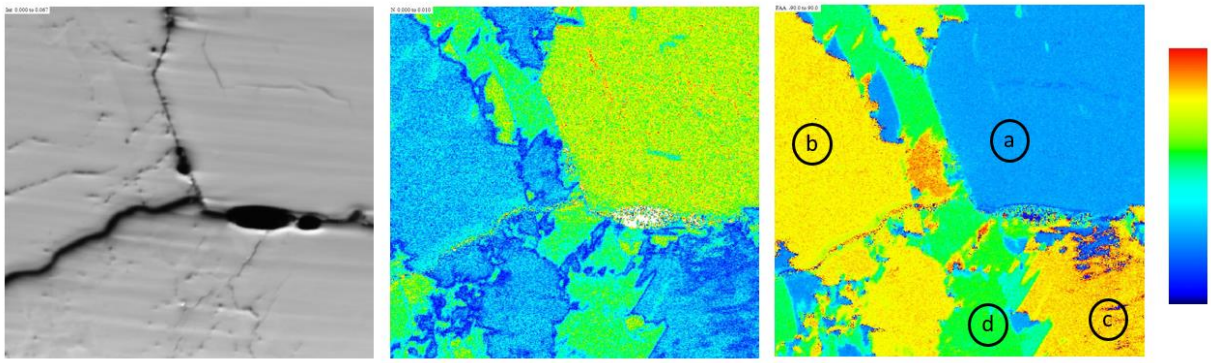

Figure 5. 2-MGEM data images of region 1 of sample c-perp. The color scale is to the right and the values in parentheses give the ranges. The scale is 2.065 X 1.960 mm.

Subregion R1a corresponded to the region also measured by X-ray Laue and EBSD. According to the Laue results, this region was aragonite with the c-axis oriented nearly normal to the surface, off by 0.7°, and the [110] was pointing down, off by 7°. The 2-MGEM results showed that the diattenuation was small but measurable. If the c-axis is precisely normal to the surface, then the diattenuation will be determined by the refractive indices for light polarized along the [100] and [010] directions. For aragonite, these refractive indices are nearly the same making the diattenuation small. Using Equations 7, N = 0.0063 (subregion R1a) and the values for n_{o1} and n_{o2} in Table 1, the birefringence in the a-b plane can be calculated to be 0.0053, which agrees with the measured values within error.

Table III The diattenuation N and direction of principal axis γ for the marked subregions shown in Figures 5, 6, and 7

	R1 N	R1 γ (°)	R2 N	R2 γ	R5 N	R5 γ (°)
a	0.0063±0.0015	-48±4	0.0053±0.0015	-13±7	0.1629±0.0015	57.2±0.2
b	0.0034±0.0015	61±8	0.0064±0.0015	-46±4	0.0062±0.0013	-48±4
c	0.0032±0.0015	58±19	0.0032±0.0015	57±9	0.0032±0.0013	54±16
d	0.0044±0.0015	4±7	0.0063±0.0015	-51±4		

Two other subregions are also visible from the 2MGEM data presented in Figure 5. Subregions R1b and R1c have the same measured N and γ, while subregion R1d has an N value intermediate between the other subregions and a different γ. The low diattenuation regions R1b and R1c have very low N values. One possible reason for this is that the c-axis in this region is tilted off-normal by ~7°±2° perpendicular to the direction of highest refractive index. (These regions were too small to be measured by our Laue system.) These data indicate that there are at least 3 different orientations of crystallites in aragonite where the c-axis is nominally pointed perpendicular to the sample surface, but have radically different orientations of the a- and b- axes.

Figure 6 shows another region of the c-perp sample in which the measured diattenuations are all small but measureable. The low intensity region shows the position of a crack in the sample which scatters light out of the collection cone of the optics. One obvious result of this is that the 2MGEM measurements are very inaccurate in this part of the sample. As with the data of Region 1 (Figure 5), there are three identifiable crystallites: high diattenuation (R2b and R2d), low diattenuation (R2c) and intermediate diattenuation (R2a).

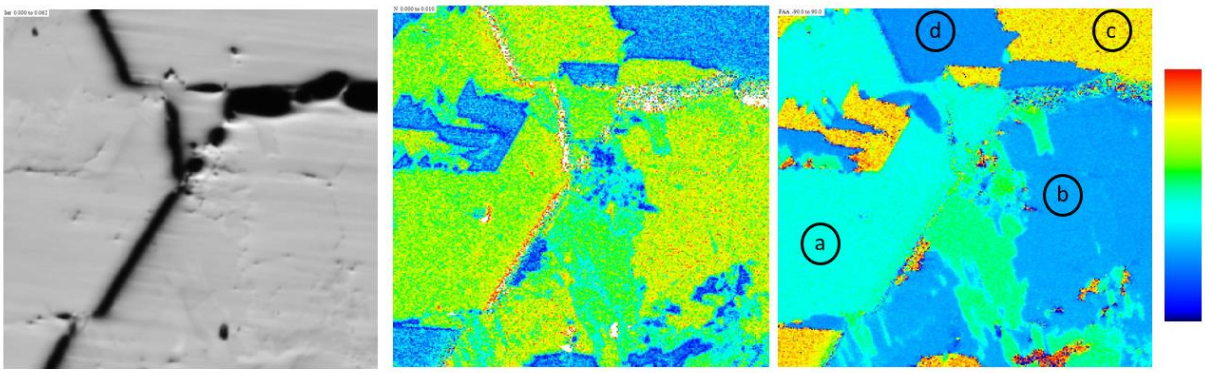

Figure 6. 2-MGEM data from sample c-perp region 2. The color scale is to the right and the values in parentheses give the ranges. The scale is 1.535 X 1.47 mm.

Figure 7 shows the 2MGEM data for region 5, which contains a feature with a very large diattenuation (subregion R5a). Using Equation 9, the c-axis angle is ~67°±2° with respect to the sample surface. The two other regions R5b and R5c have values of N that correspond to regions R1a and R1b, c respectively.

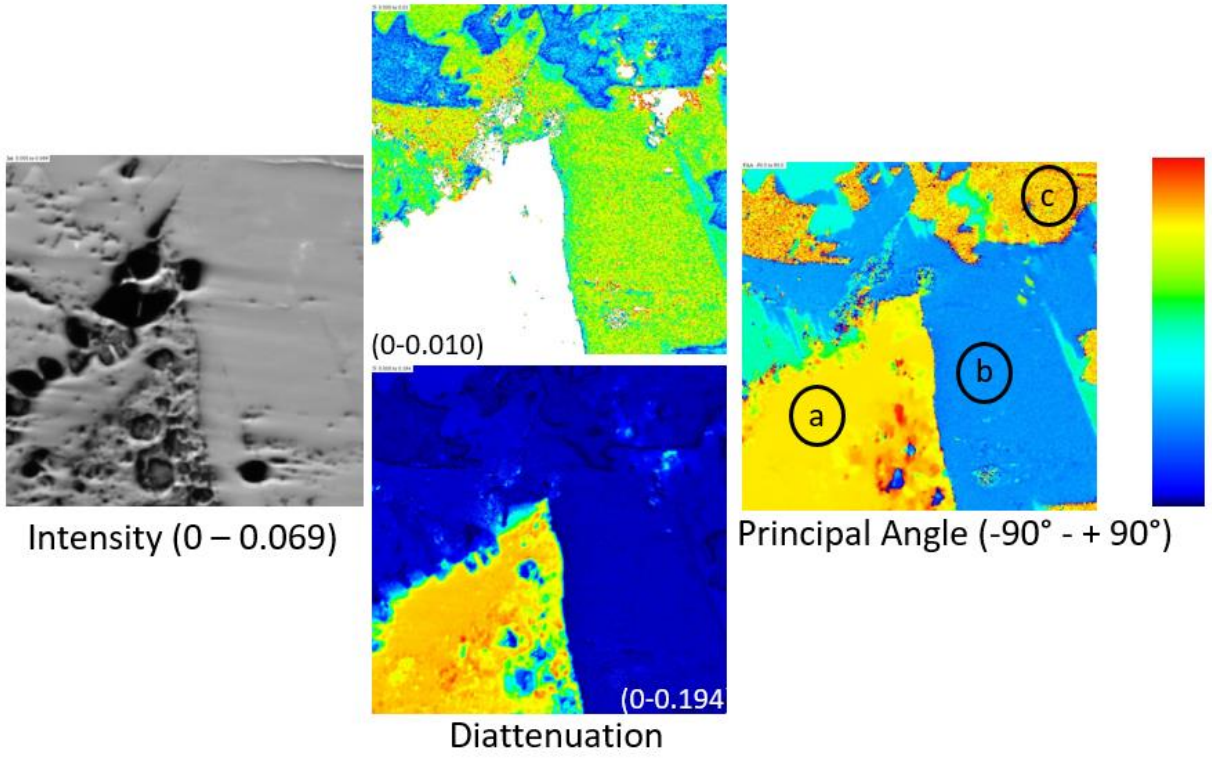

Figure 7. 2-MGEM data from sample c-perp region 5. The color scale is to the right and the values in parentheses give the ranges. The scale is 1.535 X 1.47 mm. Note that the diattenuation data is presented twice using different scales.

D. Comparisons with EBSD

Figure 8 shows a comparison between EBSD and 2-MGEM for the cperp sample region 2 (Figure 6). While the EBSD image shows significant pincushion distortion and the registration is rotated ~18° with respect to the 2-MGEM data image, both techniques provide images of the crystallites as well as their boundaries. In the EBSD image, there are several off-color dots that are the result of the inability of the software to determine the crystallographic orientation from the Kirkuchi patterns. The color patterns in the EBSD image shows that all the observed crystallites are oriented with their c-axes nearly-normal to the sample surface; this agrees with the small diattenuation observed from the 2MGEM images of the data.

EBSD data were also taken on the large diattenuation feature of region 5b, shown in Figure 6. The EBSD measured the c-axis angle as 68.9°±3.0° with respect to the sample surface; this compares well with the 2-MGEM result of 67.1°±0.7°. These results agree within the stochastic and systematic errors of the measurements.

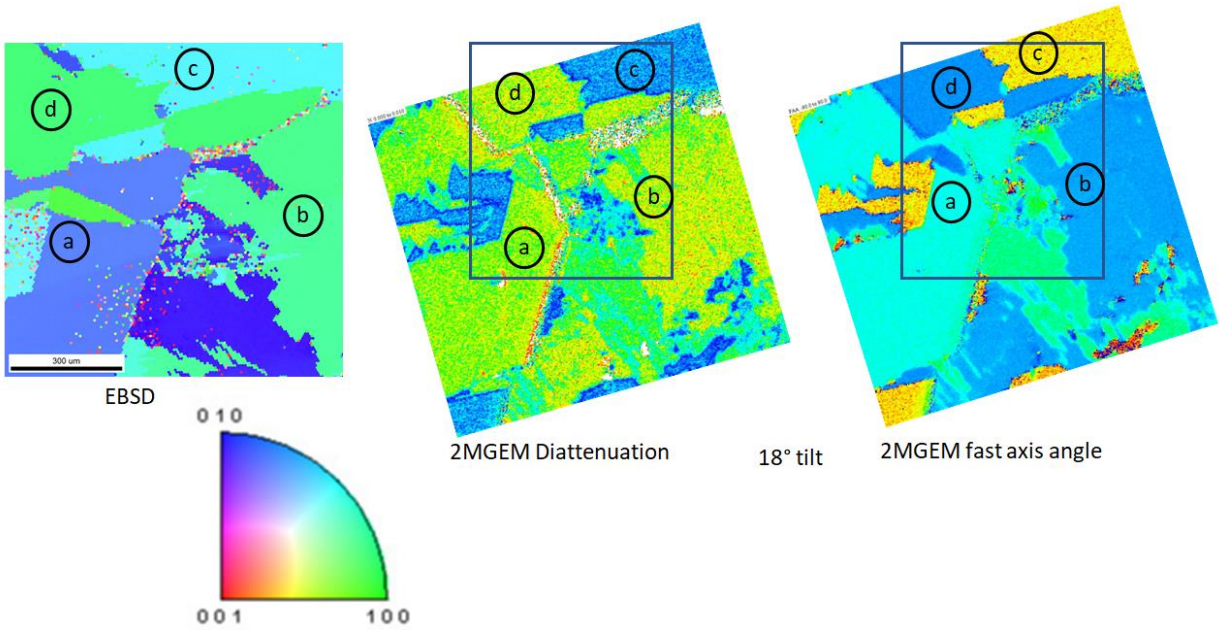

Figure 8. Comparison of 2MGEM data from region 2 and EBSD data from nearly the same region. Note that the EBSD data shows some significant pincushion distortion for such a large scan. Moreover, there is a significant registration issue in that the EBSD sample was rotated ~18° with respect to the 2MGEM data. The color code beneath the EBSD plot shows the orientation of each pixel.

Detailed comparisons of the 2-MGEM and EBSD techniques were performed on subregions R2b and R5a (Figure 9). This calculation uses Equations 6a and 6b, in which the diattenuation N and principal axis angle γ are calculated as a function of the Euler angles θ, ϕ, and ψ. The range of the calculation was: ϕ = 0° to 180° with step of 1°; ψ = 0° to 180° with step of 1°; θ = 0° to 20° with step of 0.2° for subregion R2b and θ = 0° to 90° with step of 0.5° for subregion R5a. This resulted in over 3 million calculations. If the calculated values of N and γ fall within the error-bounded experimental values, then that value of (θ, ϕ, ψ) is considered a valid value and plotted as black in Figure 9; if the calculated values of N and γ do not fall within the error-bounded experimental values, then that area is plotted as white. Thus, the black areas of Figure 9 represent the acceptable values of the Euler angles describing the crystallite orientation for a given value of N and γ, including errors. For comparison purposes, the Euler angles from the EBSD measurement are plotted as a gray ellipse, where the extent of the ellipse indicates the estimated error (both stochastic and systematic) of the EBSD measurement. While the relative errors of the EBSD and 2-MGEM instruments can be very good, both instruments are suseptable to the systematic error resulting from sample placement; it is estimated that the combined systematic error is ~3°.

Region 2b has a very small diattenuation, indicating that the c-axis is nearly perpendicular to the sample surface. However, the refractive index difference in the a and b directions can also contribute to the diattenuation. As a result, the 2-MGEM data can only say that the θ angle of the crystallite is small, and that there is some correlation between the ϕ and ψ angles. Region 5a is different, in that the 2MGEM data specifies the θ and ϕ angles but cannot determine the ψ angle. This is very similar to the results for

uniaxial calcite and dolomite analyzed by Jellison et. al (2018), where the ψ angle is degenerate. In both regions, the EBSD data agrees with an acceptable orientation of the crystallite direction from the 2-MGEM data.

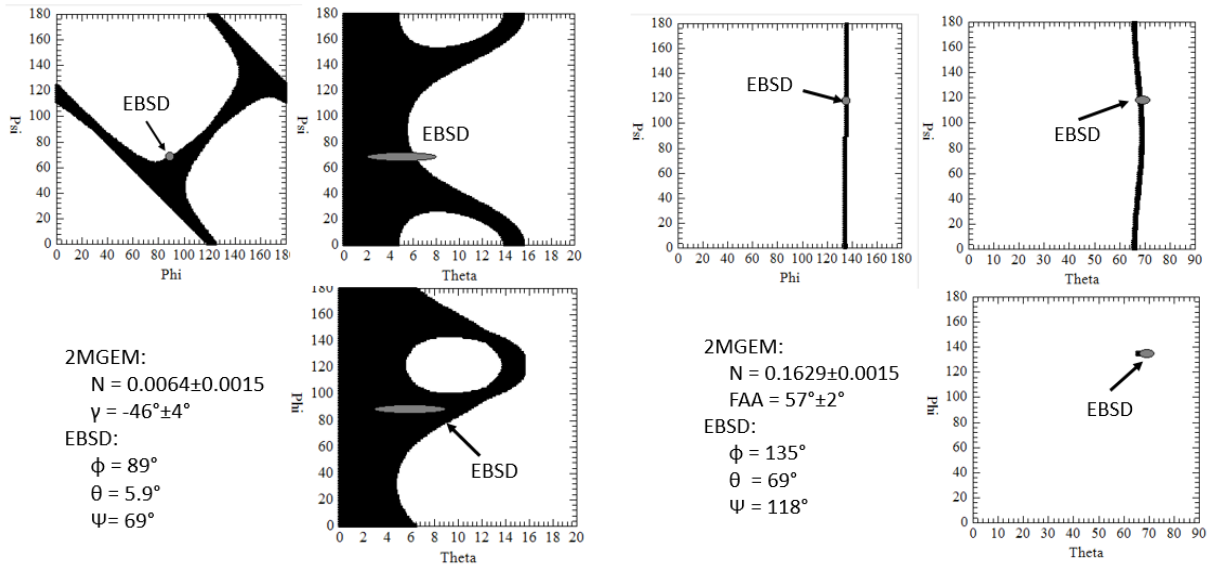

Figure 9. The possible Euler angles (Phi = ϕ, Psi = ψ,Theta = θ) for the orientation of the crystallites of subregions R2b (left) and R5a (right). See the text for a description of the calculation technique. The gray ellipse indicates the measured Euler angles from EBSD, where the extent of the ellipse indicates the estimated error, both stochastic and systematic.

V. CONCLUSIONS

The 2-modulator generalized ellipsometry microscope (2-MGEM) measures the optical diattenuation N and the direction of the principal axis γ as a function of position of a sample with an optical resolution of ~6 μm. This instrument has been used to study a natural crystal of orthorhombic aragonite ($CaCO_3$), which is a polymorph of uniaxial calcite. Since aragonite is orthorhombic, it is biaxial with a different refractive index for light polarized along each of the 3 orthogonal principal axes of the crystal. Like calcite, one refractive index is considerably smaller than the other two, making aragonite highly birefringent. The refractive indices for light polarized along the other two principal axes are nearly the same. Since aragonite is orthorhombic, it is not possible to determine the principal axes orientation from 2-MGEM measurements alone, but it is possible to place limits on the crystallographic orientation. Furthermore, since different crystallographic orientations will usually result in different values of the diattenuation and direction of the principal axis, it may be possible to use 2MGEM measurements to discern different crystallites within the sample.

If the crystal is cut such that the c-axis is nominally in the plane of the sample surface, then the diattenuation is large and the principal axis γ can be used to distinguish between different crystallites. The measurement accuracy of γ can be as good as ±0.2°, so very small angle grain boundaries can be

measured. When the crystal was cut such that the c-axis was nearly perpendicular to the sample surface, then several different crystallites could be seen, with quite different orientations of the a-b plane.

X-ray Laue and electron beam backscatter diffraction (EBSD) measurements were also made on some of the regions of these crystals that were measured using 2-MGEM. Comparisons can be made and the results agree within error.

These results along with the results of Jellison et. al (2018) show that 2-MGEM measurements are a useful tool for the examination of geological samples that contain high birefringent materials such as aragonite, calcite, and dolomite. Sample preparation is relatively simple in that only a single optically polished surface is necessary; it is not necessary to fabricate a thin section as would be required for universal stage (Berek, 1924, Emmons, 1959) or computer-integrated polarization microscopy (Panozzo-Heilbronner and Pauli, 1993). Since the measurements are in reflection, optically absorbing, opaque, or translucent samples can be examined. While EBSD measurements can be used to determine actual crystallographic orientation, they require a scanning electron microscope (SEM), must be performed in vacuum, require a thin graphite layer to avoid charging, examine only the top ~5 nm of the sample, and can be suceptable to image distortion for large area images. On the other hand, 2-MGEM measurements are performed in air, do not require any additional layer, and are not susceptible to image distortion. The depth of sample examined using the 2-MGEM is dependent on the sample, since the measurement is mostly sensitive to the magnitude of the change in refractive index with depth.

ACKNOWLEDGEMENTS

This research was supported by the U.S. Department of Energy, Office of Nuclear Energy, Light Water Reactor Sustainability (LWRS) Program, under contract DE-AC05-00OR22725 with UT-Battelle, LLC, via ORNL. Work by MC was supported by the U.S. Department of Energy, Office of Science, Office of Basic Energy Sciences, Chemical Sciences, Geosciences, and Biosciences Division. The authors acknowledge the work of Tom Geer, ORNL, for his preparation of the samples examined for this paper.

References

Berek, M., Mikroskopische Mineralbestimmung mit Hilfe det Universaldrehtischmethoden, Gebrüder Bornträger (Berlin, 1924).

Berreman, D. W. "Optics in stratified and anisotropic media: 4 X 4 matrix formulation," *J. Opt. Soc. Am.* **72**, 502-510 (1972).

Bragg, W. L., "The refractive indices of calcite and aragonite," *Proceedings of the Royal Society of London, Series A*, **105**, 370-386 (1924).

Chang, L. L. Y., Howie, R. A., and Zussman, J., "Non-silicates:sulphates, carbonates, jphosphates, halides (Rock forming minerals), 2nd edition," (Geological Society of London, 1995).

Christy, A. G., "A Review of the Structures of Vaterite: The Impossible, the Possible, and the Likely," *Crystal Growth & Design*, **17**, 3567-3578, (2017).

Davis, B. L., and L. H. Adams, "Kinetics of the calcite ⇌ aragonite transformation" *Journal of Geophysical Research,* **70,** 433-441 (1965).

Emmons, R. C., "The universal stage (with five axes of rotation)," (The Geological Society of America, (1959).

Huang, W.-L., "Synthetic polycrystalline aragonite to calcite transformation kinetics: experiments at pressures close to the equilibrium boundary,": *Mineralogy and Petrology*, **79**, 243-258, (2003).

Jellison, Jr., G. E., "Data Analysis for spectroscopic ellipsometry," *Thin Solid Films* **234**, 416-422 (1993).

Jellison, Jr., G. E. and Modine, F. A., "Two-Modulator Generalized Ellipsometry: Experiment and Calibration," *Appl. Opt.* **36**, 8184-8189 (1997); "Two-Modulator Generalized Ellipsometry: Theory," *Appl. Opt.* **36**, 8190-8198 (1997).

Jellison, Jr., G. E., "Spectroscopic ellipsometry data analysis: Measured versus calculated quantities," *Thin Solid Films* **313-314**, 33-39 (1998).

Jellison, Jr., G. E., Hunn, J. D. and Rouleau, C. M., "Normal-incidence generalized ellipsometry using the two-modulator generalized ellipsometry microscope (2-MGEM)," *Appl. Opt.***45**, 5479-5488 (2006).

Jellison, Jr., G. E., McGuire, M. A., Boatner, L. A., Budai, J. D., Specht, E. D., and Singh, D. J., "Spectroscopic dielectric tensor of monoclinic crystals: $CdWO_4$" *Phys. Rev. B* **84**, 195439 (2011).

Jellison, Jr., G. E., Leonard, D. N., Anovitz, L. M., Parish, C. M., Specht, E. D., and Rosseel, T. M., "Crystallographic orientation of uniaxial calcite and dolomite determined using reflection generalized ellipsometry," *J. Appl. Phys.* **124**, 223102 (2018).

Le Pape, Y., Tajuelo Rodriguez, E., Arregui-Mena, J'D., Giorla, A., Anovitz, L., and Rosseel, T. M., Neutron-irradiation-induced damage assessment in concrete using combined phase characterization and nonlinear and nonlinear FFT simulation, Proceedings of the 10th International Conference on Fracture Mechanics of Concrete and Concrete Structures (submitted, April 2019).

Meldrum, F. C. “Calcium carbonate in biomineralisation and biomimetic chemistry,” Int. Mater. Rev. **48**, 187-224 (2003).

Morse, J. W., Arvidson, R. S., and Lüttge, A., “Calcium carbonate formation and dissolution,” Chem. Rev. **107** 342-381 (2007).

Panozzo-Heilbronner, R. and Pauli, C. “Integrated spatial and orientation analysis of quartz c-axes by computer-aided microscopy,” J. Struct. Geol. **15**, 369-383 (1993).

Prior, D. J., Boyle, A. P., Brenker, F., Cheadle, M. C., Day, A., Lopez, G., Pernuzzo, L., Potts, G. J., Reddy, S., Spiess, R., Timms, N. E., Trimby, P. Wheeler, J., and Zetterstrom, L., “The application of electron backscatter diffraction and orientation contrast imaging in the SEM to textyural problems in rocks,” Am. Mineral. **84**, 1741-1759 (1999).

Rosseel, T. M., Gussev, M. N., Mora, L. F., “The Effects of Neutron Irradiation on the Mechanical Properties of Mineral Analogues of Concrete Aggregates,” *Proceedings of the 18th International Conference on Environmental Degradation of Materials in Nuclear Power Systems – Water Reactors*, *Vol..2* , J. H. Jackson et al., The Minerals, Metals & Materials Series, pp. 151-161 https://doi.org/10.1007/978-3-319-68454-3_14 (October 2017)

Silva, C., Rosseel, T. M., & Kirkegaard, M. C., “*Radiation-Induced Changes in Quartz, A Mineral Analog of Nuclear Power Plant Concrete Aggregates,” **Inorg. Chem., 2018,** DOI:* 10.1021/acs.inorgchem.8b00096

Troeger, W. E., “Optical determination of rock-forming minerals, Part 1:Determinative Tables” (Lubrecht & Cramer Ltd, 1979).